Morphology and dynamics of Venus oxygen airglow from Venus Express/Visible and Infrared Thermal Imaging Spectrometer observations

R. Hueso, Agustín Sánchez-Lavega, Giuseppe Piccioni, Pierre Drossart, Jean-Claude Gérard, Igor V. Khatuntsev, Ludmilla Zasova, Alessandra Migliorini

Morphology and dynamics of Venus oxygen airglow from Venus Express/Visible and Infrared Thermal Imaging Spectrometer observations

R. Hueso,[1] A. Sánchez-Lavega,[1] G. Piccioni,[2] P. Drossart,[3] J. C. Gérard,[4] I. Khatuntsev,[5] L. Zasova,[5] and A. Migliorini[2]

Received 21 January 2008; revised 21 March 2008; accepted 2 May 2008; published 26 July 2008.

[1] Images obtained by the Visible and Infrared Thermal Imaging Spectrometer (VIRTIS)-M channel instrument onboard Venus Express have been used to retrieve maps and apparent motions of the O_2 ($^1\Delta$) infrared nightglow on Venus at 1.27 μm. The nightglow distribution is highly inhomogeneous with the regions of brightest emission generally located at low latitudes near the midnight meridian. Unexpectedly some orbits show also intense airglow activity over the south polar region. The spatially resolved airglow is spectacularly variable not only in its morphology and intensity but also in the apparent motions of the airglow small- and large-scale structures. Visual tracking of the bright features allowed to obtain mean zonal and meridional motions related to the subsolar to antisolar circulation. The zonal velocity is dominated by an intense prograde jet (contrary to the retrograde planetary rotation) from dawn to midnight extending up to 22 hours in local time with lower velocities and reversed sign from dusk. Typical zonal velocities range between +60 (prograde) to −50 (retrograde) m/s, whereas most meridional velocities range from −20 (poleward) to +100 m/s (equatorward) with an average meridional circulation of +20 m/s toward low latitudes. The brightest small-scale (∼100 km) features appear correlated with locations of apparent convergence which may be a signature of compression and downwelling, whereas this is not evident for the large-scale structures suggesting slow subsidence over large areas mixed with horizontal motions. We argue that part of the tracked motions are representative of real motions at the mesosphere over an altitude range of 95–107 km.

Citation: Hueso, R., A. Sánchez-Lavega, G. Piccioni, P. Drossart, J. C. Gérard, I. Khatuntsev, L. Zasova, and A. Migliorini (2008), Morphology and dynamics of Venus oxygen airglow from Venus Express/Visible and Infrared Thermal Imaging Spectrometer observations, *J. Geophys. Res.*, *113*, E00B02, doi:10.1029/2008JE003081.

1. Introduction

[2] The circulation of the upper atmosphere of Venus is traditionally decomposed into two distinct flow patterns at different altitudes: A subsolar-to-antisolar (SS-AS) thermospheric circulation cell driven by solar heating, stable at levels above the mesosphere (z > 120 km [*Bougher et al.*, 1997], and a superrotating zonal (SZ) flow in the planetary rotation sense at the upper troposphere (z ∼ 65 km) [see, e.g., *Gierasch et al.*, 1997; *Markiewitz et al.*, 2007; *Limaye*, 2007; *Sánchez-Lavega et al.*, 2008]. In the transition region, the mesosphere (70 < z < 120 km), the interaction of both motions results in a complex circulation that greatly varies over time [*Lellouch et al.*, 1997; *Bougher et al.*, 2006]. The global circulation in the mesosphere is probably influenced by a number of physical processes such as breaking gravity waves [*Alexander*, 1992] and diffusive processes, but their effects over the mesospheric circulation are not well understood or quantified [*Bougher et al.*, 2006]. Additionally, the return branch of the SS-AS upper circulation must lie somewhere in the mesosphere but its location has not been clearly identified.

[3] While the dynamics of the mesosphere of Venus is hardly accessible to in situ measurements it can be studied by means of Doppler shifts in certain absorption lines sensitive to mesospheric levels [e.g., *Clancy et al.*, 2007; *Widemann et al.*, 2007] but this technique lacks spatial resolution, requires a sophisticated analysis of the observations and a precise treatment of systematic errors. A complimentary technique suited for exploration from a spacecraft is the study of nightglow molecular emissions which trace the motions of different chemical species in the

[1] Departamento de Física Aplicada I, E.T.S. Ingenieros, Universidad del País Vasco, Bilbao, Spain.
[2] Istituto di Astrofisica Spaziale e Fisica Cosmica, INAF-IASF Roma, Rome, Italy.
[3] Laboratoire d' Etudes Spatiales et d' Instrumentation en Astrophysique, Observatoire de Paris, Université Paris-Diderot, CNRS, UPMC, Meudon, France.
[4] Laboratoire de Physique Atmosphérique et Planétaire, Université de Liège, Liège, Belgium.
[5] Space Research Institute, Moscow, Russia.

0148-0227/08/2008JE003081

upper atmosphere with the drawback that the emissions are coupled with photochemical processes.

[4] Among the many nonthermal emissions produced in Venus, the oxygen airglow at 1.27 μm is the most intense. Its was first detected in ground-based observations of Venus by *Connes et al.* [1979]. This airglow is produced by the recombination of oxygen atoms dissociated by photolysis of CO_2 at thermospheric altitudes on the sunlit hemisphere. In the upper mesosphere (95–110 km) three-body recombination of O atoms leads to O_2 formation in a particular excited state, $a^1\Delta_g$, which is followed by airglow emission as the molecule relaxes to its $X^3\Sigma_g^-$ ground state. The radiative lifetime of O_2 singlet state is ~70 min. [*Lellouch et al.*, 1997; *Miller et al.*, 2001]. The O_2 airglow is observed in the night-side hemisphere at 1.267 microns [*Allen et al.*, 1992; *Bougher and Borucki*, 1994] and with far less intensity in O_2 Herzberg II visible wavelengths [*Krasnopolsky et al.*, 1976; *Bougher et al.*, 1997].

[5] It was soon realized that the intense oxygen IR nightglow is highly variable from day to day [*Crisp et al.*, 1996], its intensity distribution is generally not symmetric in latitude [*Allen et al.*, 1992], often exhibits multiple local maxima, and shows variations on timescales as short as 1 hour [*Lellouch et al.*, 1997]. The related nitric oxide nightglow emission was mapped during the Pioneer Venus mission [*Stewart et al.*, 1980] statistically presenting larger brightness close to the Equator and shifted by about 2 hours from midnight toward dawn. Both nightglows are decoupled in height providing information about different vertical levels: 95–105 km for O_2 airglow (G. Piccioni et al., Venus oxygen airglow vertical profile, submitted to *Journal of Geophysical Research*, 2008) and ~115 km for NO [*Gérard et al.*, 2008b].

[6] In this work we have used night side nadir observations from the Visible and Infrared Thermal Imaging Spectrometer (VIRTIS) [*Drossart et al.*, 2007a] on board the Venus Express orbiter [*Titov et al.*, 2006; *Svedhem et al.*, 2007] to construct maps of the Venus atmosphere in the O_2 emission band. The airglow maps were used to study the morphology and temporal variability of the airglow. In those orbits where the airglow is particularly intense we also measured the displacement of "cloud-like" airglow features.

[7] Preliminary measurements of apparent motions were presented by *Drossart et al.* [2007b] for selected orbits. *Gérard et al.* [2008a] gave a precise account of the average distribution of the O_2 nightglow. Other works in this special section (Piccioni et al., submitted manuscript, 2008) present results obtained in limb view which lead to vertical profiles of the airglow emission.

2. Observations and Methods

[8] We analyzed data obtained during 28 consecutive orbits between 1 July 2006 and 28 July 2006, one orbit on 6 August 2006 presenting a good view of the equator, six orbits between December 2006 and January 2007 and five orbits from 7 April 2007 to 11 April 2007 that cover the polar region in higher detail than the rest of the VIRTIS data set. The data were selected according to the availability of high-resolution observations, fast repetition in each orbit (two or more images of the same region separated by 1hour) and the strong airglow emission present during most of the selected orbits. The Sun F10.7 flux (a convenient measurement of the solar activity in radio wavelengths commonly used as a proxy of the Sun's irradiance in the Extreme UltraViolet) averaged over July 2006, August 2006, January 2007 and April 2007 was 76×10^{-22}, 79×10^{-22}, 84×10^{-22} and 72×10^{-22} W/m^2 Hz respectively, reflecting homogeneous conditions for the Sun's activity close to the solar minimum.

[9] Oxygen airglow at 1.27 μm superimposes with thermal radiation coming from the lower atmosphere and partially filtered by the lower clouds. In order to subtract the thermal contribution from the total airglow signal we compare VIRTIS fluxes measured in the 1.26–1.28 μm wavelength range to the flux on the 1.18 μm observation window which provides a nearby region with flux dominated by the lower thermal emission. In addition, O_2 photons emitted downward are subsequently backscattered by the underlying clouds and enhance the measured airglow radiation. A correction factor of 2.7 was used for nadir observations and geometry effects were corrected to first order by multiplying each pixel by the cosine of the emission angle [*Crisp et al.*, 1996]. This crude estimation of brightness emission is adequate for VIRTIS observations of subpolar and midlatitudes (emission angles lower than 40°) but may fail in the few observations containing information about the tropics and the equator. Finally, depending on the latitudes being sampled we projected the images in longitude-latitude maps or polar stereographic projections to compare images obtained from different observational geometries.

[10] Images separated by 1 hour allowed to track and retrieve the displacements of the airglow features in 23 of the 40 orbits, typically the orbits with higher intensity airglow structures, being the remaining orbits characterized by low intensity of the airglow or low contrast of the observed structures. The apparent motions of distinct airglow features were measured visually using the PLIA software [*Peralta et al.*, 2005].

3. Morphology of the Oxygen Airglow and Temporal Variability

3.1. Low and Mid Latitudes

[11] As a consequence of the quasi-polar VEX orbit, the airglow activity at low latitudes is only partially covered by VIRTIS observations with a resolution of 100 km pix^{-1} in some cases, while mid to subpolar latitudes are observed on many orbits with spatial resolution down to 15 km pix^{-1}.

[12] The statistical distribution of Venus oxygen nightglow is inhomogeneous with the regions of brightest emission located at low latitudes near and dawnward of the midnight meridian [*Gérard et al.*, 2008b]. Maps of airglow brightness distribution of different regions are presented in Figure 1 using data from orbits that sample nearly simultaneously most of the Southern Hemisphere. On this data set the equatorial region at midnight always presents high values of brightness. Large structures with typical sizes of ~3000 km extending from the equator to midlatitudes are often observed. In most cases the large-scale structures observed on Figure 1a are similar to the global structures seen in the global map of airglow brightness presented by *Gérard et al.* [2008a] and constructed by averaging several

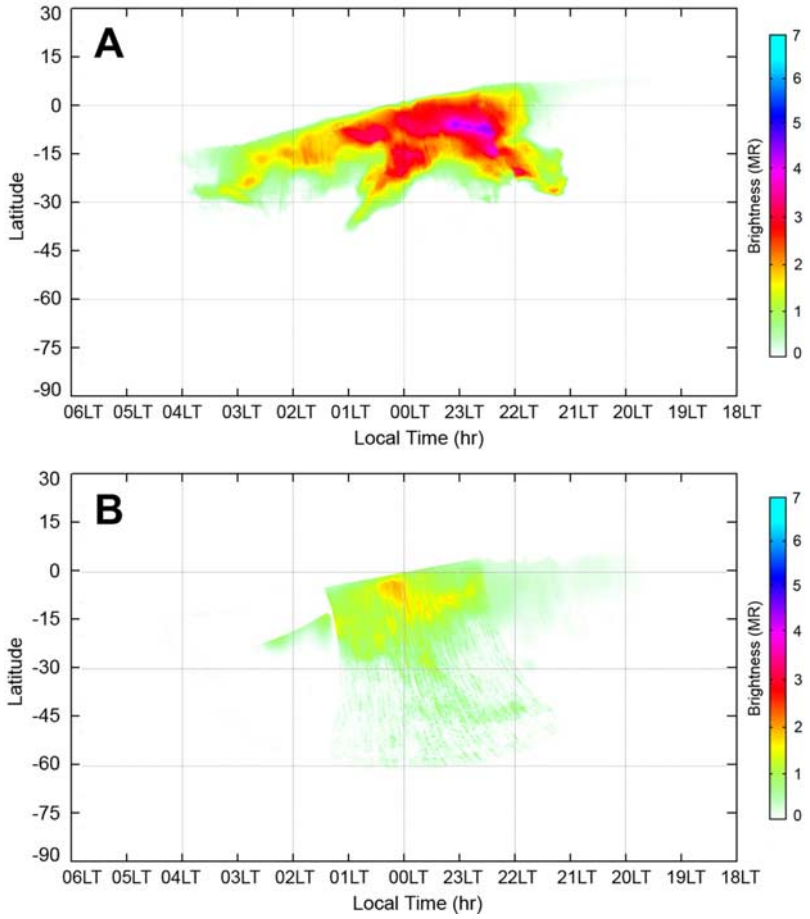

Figure 1. Airglow intensity map obtained during orbits (a) 87 (16 July 2006) and (b) 91 (20 July 2006). The wide coverage of the maps is close to half the night-side hemisphere and was obtained using data from three different VIRTIS data cubes for each map. The mean brightness of the sampled regions close to the equatorial midnight can change from 5 MR to 1 in a single day but the large values are more common.

hundred maps from different dates. Remarkably, though largely expected, the mean airglow brightness in VIRTIS images (centered at the same latitude and local time and covering areas as big as 1.5×10^7 km^2) changes dramatically from one orbit to other. Changes observed on Figure 1 are sometimes observed on timescales as short as 1 day over the VIRTIS data set. On the contrary, large-scale structures as seen on Figure 1a are stable on timescales of 2 hours or longer indicating sustained formation of excited oxygen molecules.

3.2. Polar Latitudes

[13] *Gérard et al.* [2008a] give an average value of O_2 airglow brightness at ~70°S of ~1.2 MegaRayleighs (MR). In contrast, intense airglow activity can also arise over polar latitudes in particular orbits. This was unexpected since the polar regions are far from the antisolar point and should contain lower densities of oxygen atoms. Figure 2 shows two images of a sequence of VIRTIS observations of the most intense airglow brightness over polar latitudes and viewed with an emission angle lower than 20° for all the sequence. A gaussian fit to the brightness temporal evolution of this structure following its motion gives a time decay of 3 hours with a peak brightness of 7 MR over a 100 km elongated structure, moving toward lower latitudes with a meridional velocity of $v = 50 \pm 10$ m/s. The brightness decay in time of this structure was about 2.5 times the radiative lifetime of the oxygen airglow indicating continuous production of excited molecules over this small region.

[14] The period from 7 to 11 April 2007 was used for detailed research of the polar area finding intense airglow activity in all the VIRTIS images and sustained during all orbits. Figure 3 shows a sequence of observations where apparent motions of the airglow lead to a polar to low latitudes apparent motion with $v \sim 50 \pm 5$ m/s. Detailed motions in the whole movie during this orbit (composed of 12 images at time steps of 30 min to 1 hour) shows that the airglow evolves by a combination of apparent motions at small scale and activation and deactivation of airglow emission structures over extended regions.

4. Apparent Motions and Mesospheric Circulation

[15] Figure 4 shows apparent motions tracked over airglow structures on different dates, latitudes and local times. The panels show that the morphology of the airglow is related with the apparent motions tracked. Large-scale

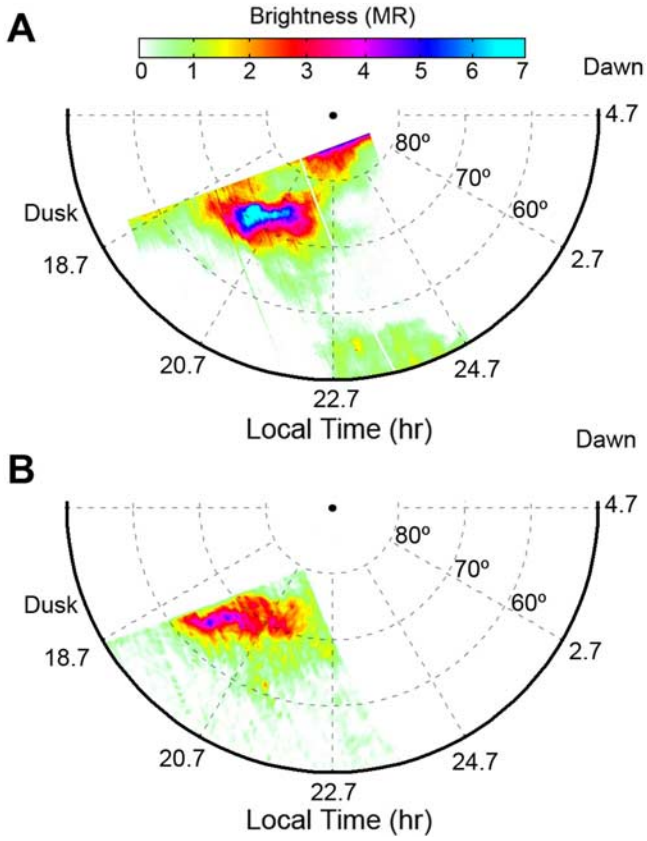

Figure 2. Polar projections and time evolution of the brightest airglow structure seen on polar latitudes. Longitudes are given in terms of local times. Observations correspond to orbit 80, 9 July 2006, and the time difference between both observations is 3 hours.

structures move slowly on one direction (generally perpendicular to the airglow brightness front) while smaller-scale structures move more rapidly in the direction defined by the front (see Figure 4a).

[16] The equatorial region covered on Figure 4d looks turbulent with bright features colliding suggesting that the observed motions may come from a variety of different altitude levels. Some of the brightest structures (notably on Figure 4e, but also on Figures 4c and 4d and particular regions on Figure 4a) correlate with locations where convergence of the apparent motions is present. This behavior may not apply to the larger-scale structures, since they appear surrounded by far less intense airglow features and thus, it is not possible to retrieve motions around them.

[17] Figure 5 shows the mean horizontal circulation in Venus' night-side hemisphere obtained by spatially and temporally averaging the ensemble of apparent motions obtained in 23 orbits with ~1000 tracked motions. The upper part of Figure 5 also shows the local time-latitude location of the specific regions displayed in Figure 4. The large variability in intensity and direction of the velocities, which sometimes can be as high as 100 m/s, results in low values of the average speeds. The most remarkable feature in this plot is a repeatedly observed jet at 35°S with an average zonal speed of $u = 30$ m/s opposite to the planetary rotation and with motions twice as intense in the early morning hours (0600 0200 local time) and reversed in direction from 1800 to 2000 local time. The meridional motions are more intense at subpolar latitudes (70°S) with average velocities of $v \sim 20$ m/s, decreasing toward lower latitudes and reaching a minimum value of $v \sim 5$ m/s at 15°S and increasing again at equatorial latitudes.

[18] In the orbits with high intensities of the airglow emission (notably on the equatorial case and the five polar orbits) the displacements of the airglow brightness patterns seem to take place at different altitude levels since the images show a mixture of structures moving with different speeds that visually seem to superimpose. In support of this interpretation, limb observations of airglow activity some-

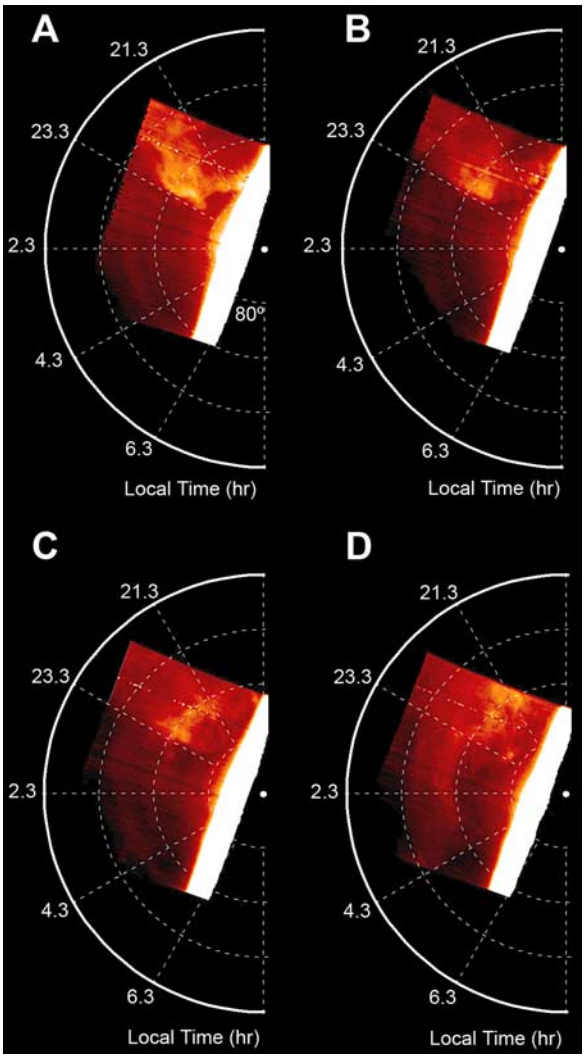

Figure 3. Polar projections and time evolution of the 1.267 μm radiance over orbit 355 obtained on 27 August 2007 at local times: (a) 1539, (b) 1739, (c) 1939, and (d) 2209. The brightest airglow features have an intensity of 1.8 MR on the first image and longitudes are given in terms of local times. The global apparent motions are toward higher latitudes. Some of the structures like the bright arm at 68°S in Figure 3d appear suddenly and are not related with horizontal motions but with the sudden airglow brightening of new regions.

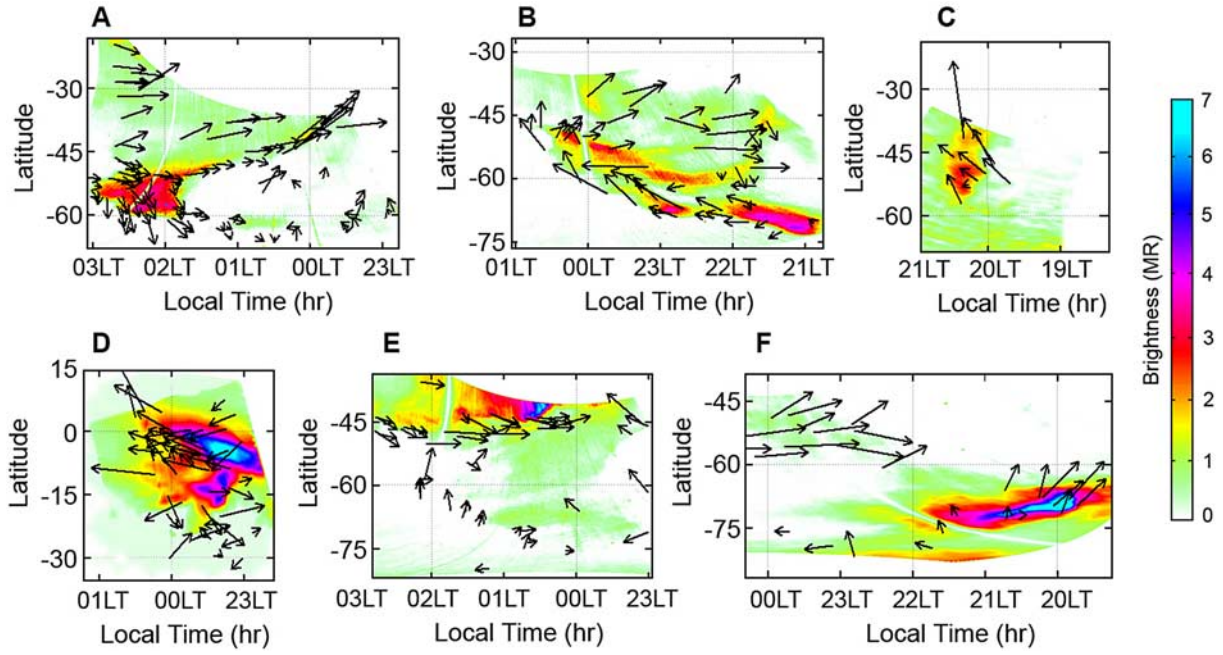

Figure 4. Average apparent motions and correlation with the airglow intensity for selected orbits: (a) orbit 96 obtained on 25 July 2006; (b) orbit 99 obtained on 28 July 2006; (c) orbit 76 obtained on 5 July 2006; (d) orbit 108 obtained on 6 August 2006; (e) orbit 84 obtained on 13 July 2006; and (f) orbit 80 obtained on 9 July 2006. The maps cover a significant portion of the local time-latitude plane showing repeatedly observed motions, like the zonal jet at 30°S–45°S opposite to the planetary rotation (Figures 4a, 4b, 4e, and 4f). Opposite motions between 45°S and 75°S that seem part of a close circulation are observed at different local times on different orbits (Figure 4b); meridional motions are toward the pole (Figure 4a) but generally directed toward low latitudes (Figures 4a, 4b, 4c, and 4f). The few observations of the equator show chaotic motions with a mean prograde (in the planetary rotation sense) component (Figure 4d). Brightness emission given are only approximative for Figure 4d with emission angles ~70°.

times presents peaks at two different altitude levels, one at 96 ± 1 km altitude and a second peak at 103–107 km altitude (Piccioni et al., submitted manuscript, 2008).

5. Discussion

[19] The average motions obtained are in agreement with a subsolar to antisolar circulation at the IR oxygen airglow levels (~96 km) with evident meridional motions from polar to low latitudes and large variability of the zonal and meridional components.

[20] Caution must be taken in interpreting the airglow brightness patterns displacements as tracers of flow motions in the lower mesosphere. They could be influenced by the activation and/or deactivation of airglow emission at specific regions by other phenomena (i.e., gravity waves affecting atmospheric density, localized or extended regions of downwelling, atmospheric diffusivity, etc).

[21] An additional level of complexity is introduced by the radiative lifetime (70 min) of the O_2 singlet state which introduces difficulties in the interpretation of the observed rates of brightness variation. The e-folding time constant of any local change (decrease or increase) cannot be less than 70 min without advection of air masses containing different proportion of glowing O_2 molecules. For airglow brightness decreasing more slowly the brightness reduction could be caused by a combination of horizontal transport and a decrease of the flux of O atoms modifying the local O density and airglow brightness. In those locations where the airglow intensity increases there must be enhanced downward flux of O atoms.

[22] The observations show two types of behavior for the Venus oxygen airglow temporal evolution. On the one hand, the large-scale 1000–3000 km structures survive at least for a few hours (longer than the radiative decay time) but change dramatically from day to day. Since limb scans of O_2 emission slightly depend on latitude with higher latitudes characterized by higher altitudes of the airglow (Piccioni et al., submitted manuscript, 2008) these large structures may descend progressively as they travel from polar latitudes to the equator, compressing and increasing the concentration of free O atoms. On the other hand, small-scale bright structures with smaller scales (100 km) seem related with the apparent convergence of motions tracked in the airglow. In fact, the time evolution of the airglow maps seems composed of two types of motions, the large-scale structures moving like "fronts" or waves, and the bright structures immersed on them or isolated, apparently moving like passive tracers. We argue that at least part of the later motions are real motions at the mesosphere as the newly formed oxygen molecules are advected by the mesospheric circulation.

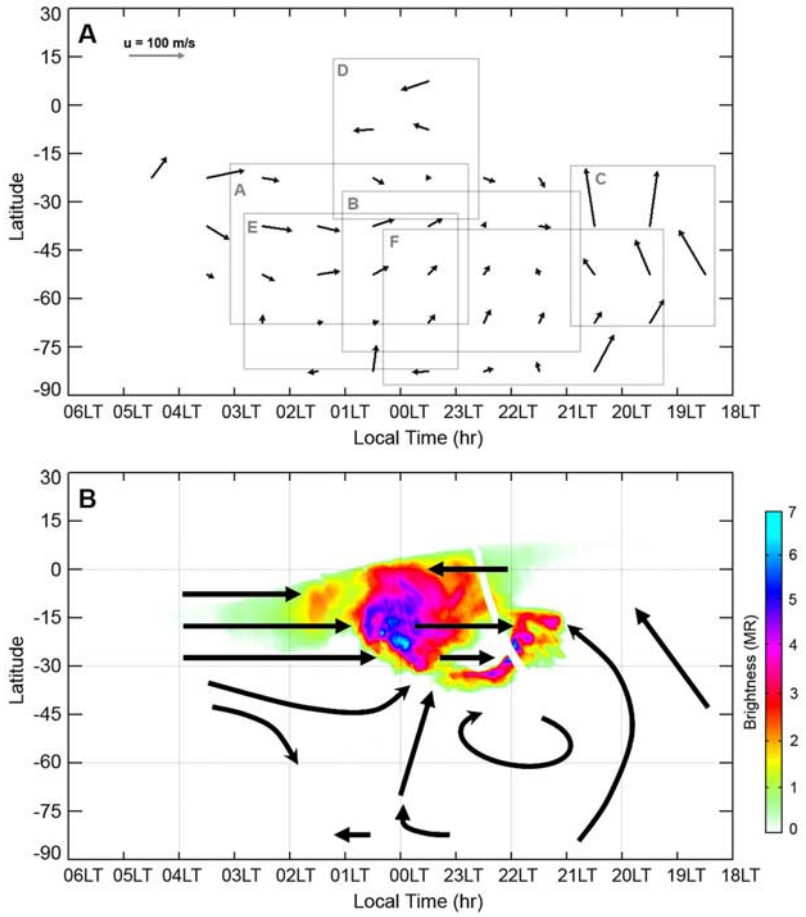

Figure 5. Mean apparent circulation of the mesospheric oxygen airglow brightness. (a) Averages of all apparent motions tracked on the airglow and also marks the sampled regions appearing on Figure 4. A reference vector of 100 m/s is included on the upper left corner of the map. (b) A schematic model of the mean circulation of Venus mesosphere from these measurements. The background image corresponds to a map of airglow brightness obtained on orbit 93, 22 July 2007, that can be compared with those on Figure 1. Regions with no arrows indicate regions with not much available data. The apparent rotating motions indicated at 50°S are found at a variety of local times depending on the particular orbit. The jet from dawn to midnight is a repetitive structure while the jet from dusk to midnight is less regular from one orbit to another.

[23] The brightest airglow patches may be regions of strong subsidence (and local adiabatic warming) associated with downdrafts that increase the volume concentration of O atoms. If this is correct, spectral maps of the O_2 IR nightglow should show a positive correlation between the brightness and the rotational temperature of the emission line. Partial confirmation of this point comes from stellar occultation experiments performed by Venus Express [*Bertaux et al.*, 2007] which result on warm temperatures at the airglow emission levels (95–100 km). Ground-based observations have been made to correlate the rotational temperature and brightness with results sometimes indicating such a correlation [*Ohtsuki et al.*, 2005] and sometimes not with some dependence on the morphology of the airglow region [*Bailey et al.*, 2007].

[24] Although the present work does not fully disentangle the different contributions to the airglow variability and therefore is not able to fully retrieve the mesospheric true motions it does show that such an approach is possible. VIRTIS-M observations obtained with shorter time differences than the radiative lifetime of the oxygen airglow (70 min) will partially help to solve this problem. Although part of the airglow motions tracked on this work were obtained on image pairs separated by 30 min the short time difference between the images translate into larger errors in the derived motions and most of the data corresponds to images separated by 1 hour. Both data sets produce similar results on terms of the mean derived circulation.

[25] Further analysis should concentrate on identifying any correlation between local temperature anomalies and O_2 intensities. Also, detailed comparison with Venus GCMs should allow to better constrain the role of gravity waves as drivers of the airglow variability. The Venus Express Extended mission should run during 2008–2009 with higher levels of solar activity. According to NOAA Space Weather Prediction Center (SWPC) a reasonable estimate is an increase of a ~60% of the F10.7 index for the end of 2009 (http://www.sec.noaa.gov/SolarCycle/SC24). This

will allow a higher airglow activity and a better sampling of Venus mesosphere through its spatial distribution and variability.

[26] Over the next years the combination of results from Venus Express instruments (VIRTIS O_2 IR maps, SPICAV thermal profiles and NO nightglow observations, VeRa thermal data combined with cyclostrophic balance over mid to high latitudes and cloud top wind tracking with VMC and VIRTIS) and ground-based observations (nightglows and Doppler winds retrieval) will allow a significant improvement of our understanding of the mesospheric dynamics and the underlying mechanisms driving its variability.

[27] **Acknowledgments.** Venus Express is a mission of the European Space Agency. We gratefully thank all members of the ESA Venus Express project and of the VIRTIS technical team. This work has been funded by Spanish MEC AYA2003-03216, with FEDER support and Grupos UPV 15946/2004 and is supported by the CNES and ASI national space agencies. R.H. acknowledges a Ramón y Cajal contract from MEC. J.C.G. acknowledges funding from the Belgian Fund for Scientific Research and the PRODEX program managed by the European Space Agency with the help of the Belgian Federal Space Science Office.

References

Alexander, M. J. (1992), A mechanism for the Venus thermospheric superrotation, *Geophys. Res. Lett.*, *19*, 2207–2210.

Allen, D., D. Crisp, and V. S. Meadows (1992), Variable oxygen airglow on Venus as a probe of atmospheric dynamics, *Nature*, *359*, 516–519.

Bailey, J. A., V. S. Meadows, S. Chamberlain, A. Simpson, and D. Crisp (2007), Variability of the Venus Oxygen Airglow, *Bull. Am. Astron. Soc.*, *38*, 526.

Bertaux, J. L., et al. (2007), A warm layer in Venus' cryosphere and high-altitude measurements of HF, HCl, H_2O and HDO, *Nature*, *450*, 646–649.

Bougher, S. W., and W. J. Borucki (1994), Venus O_2 visible and IR nightglow: Implications for lower thermosphere dynamics and chemistry, *J. Geophys. Res.*, *99*, 3759–3776.

Bougher, S. W., M. J. Alexander, and H. G. Mayr (1997), Upper atmosphere dynamics: Global circulation and gravity waves, in *Venus II: Geology, Geophysics, Atmospheres, and Solar Wind Environment*, edited by S. W. Bougher, D. M. Hunten, and R. J. Philips, Univ. of Ariz. Press, Tucson.

Bougher, S. W., S. Rafkin, and P. Drossart (2006), Dynamics of the Venus upper atmosphere: Outstanding problems and new constraints expected from Venus Express, *Planet. Space Sci.*, *54*, 1371–1380.

Clancy, R. T., B. J. Sandor, and G. H. Moriarty-Schieven (2007), Dynamics of the Venus upper atmosphere: Global-temporal distribution of winds, temperature, and CO at the Venus mesopause, *Bull. Am. Astron. Soc.*, *39*, abstract 61.07.

Connes, P., J. F. Noxon, W. A. Traub, and N. P. Carleton (1979), O_2 ($^1\Delta$) emisssion in the day and night airglow of Venus, *Astrophys. J.*, *233*, L29–L32.

Crisp, D., V. S. Meadows, B. Bézard, C. deBergh, J.-P. Maillard, and F. P. Mills (1996), Ground-based near-infrared observations of the Venus nightside: 1.27 μm O_2 ($a^1\Delta g$) airglow from the upper atmosphere, *J. Geophys. Res.*, *101*, 4577–4594.

Drossart, P., et al. (2007a), Scientific goals for the observation of Venus by VIRTIS on ESA/Venus express mission, *Planet. Space Sci.*, *55*, 1653–1672.

Drossart, P., et al. (2007b), Venus upper atmospheric emissions from VIRTIS spectral imaging observations, *Nature*, *450*, 641–645.

Gérard, J.-C., A. Saglam, G. Piccioni, P. Drossart, C. Cox, S. Erard, R. Hueso, and A. Sánchez-Lavega (2008a), Distribution of the O_2 infrared nightglow observed with VIRTIS on board Venus Express, *Geophys. Res. Lett.*, *35*, L02207, doi:10.1029/2007GL032021.

Gérard, J.-C., C. Cox, A. Saglam, J.-L. Bertaux, E. Villard, and C. Nehmé (2008b), Limb observations of the ultraviolet nitric oxide nightglow with SPICAV on board Venus Express, *J. Geophys. Res.*, doi:10.1029/2008JE003078, in press.

Gierasch, P. J., et al. (1997), The general circulation of the Venus atmosphere: An assessment, in *Venus II: Geology, Geophysics, Atmosphere, and Solar Wind Environment*, edited by S. W. Bougher, D. M. Hunten, and R. J. Philips, pp. 459–500, Univ. of Ariz. Press, Tucson.

Krasnopolsky, V. A., A. A. Krysko, V. N. Rogachev, and V. A. Parshev (1976), Spectroscopy of the Venus night airglow from the Venera 9 and 10 satellites, *Cosmic Res.*, *14*, 789–795.

Lellouch, E., T. Clancy, D. Crisp, A. Kliore, D. Titov, and S. W. Bougher (1997), Monitoring of mesospheric structure and dynamics, in *Venus II: Geology, Geophysics, Atmospheres, and Solar Wind Environment*, edited by S. W. Bougher, D. M. Hunten, and R. J. Philips, pp. 295–324, Univ. of Ariz. Press, Tucson.

Limaye, S. S. (2007), Venus atmospheric circulation: Known and unknown, *J. Geophys. Res.*, *112*, E04S09, doi:10.1029/2006JE002814.

Markiewitz, W. J., D. V. Titov, S. S. Limaye, H. U. Keller, N. Ignatiev, R. Jaumann, N. Thomas, H. Michalik, R. Moissl, and P. Russo (2007), Morphology and dynamics of the upper cloud layer of Venus, *Nature*, *450*, 633–635.

Miller, H. C., J. E. McCord, J. Choy, and G. D. Hager (2001), Measurement of the radiative lifetime of O_2 ($a^1\Delta_g$) using cavity ring down spectroscopy, *J. Quant. Spectrosc. Radiat. Transfer*, *69*, 305–325.

Ohtsuki, S., N. Iwagami, H. Sagawa, Y. Kasaba, M. Ueno, and T. Imamura (2005), Ground-based observation of the Venus 1.27-μm O_2 airglow, *Adv. Space Res.*, *36*, 2038–2042.

Peralta, J., R. Hueso, N. Barrado, and A. Sánchez-Lavega (2005), Introducing PLIA: The planetary laboratory for image analysis, *Bull Am. Astron. Soc.*, *37*, 653.

Sánchez-Lavega, A., et al. (2008), Variable winds on Venus mapped in three dimensions, *Geophys. Res. Lett.*, *35*, L13204, doi:10.1029/2008GL033817.

Stewart, A. I. F., J. C. Gerard, D. W. Rusch, and S. W. Bougher (1980), Morphology of the Venus ultraviolet night airglow, *J. Geophys. Res.*, *85*, 7861–7870.

Svedhem, H., et al. (2007), Venus Express—The first European mission to Venus, *Planet. Space Sci.*, *55*, 1636–1652.

Titov, D. V., et al. (2006), Venus Express science planning, *Planet. Space Sci.*, *54*, 1279–1297.

Widemann, T., E. Lellouch, and A. Campargue (2007), New wind measurements in Venus' lower mesosphere from visible spectroscopy, *Planet. Space Sci.*, *55*, 1741–1756.

P. Drossart, Laboratoire d' Etudes Spatiales et d' Instrumentation en Astrophysique, Observatoire de Paris, Université Paris-Diderot, CNRS, UPMC, 5 place Jules Janssen, F-92195 Meudon, France. (pierre.drossart@obspm.fr)

J. C. Gérard, Laboratoire de Physique Atmosphérique et Planétaire, Université de Liège, 5 Avenue de Cointe, B-4000 Liège, Belgium. (jc.gerard@ulg.ac.be)

R. Hueso and A. Sánchez-Lavega, Departamento de Física Aplicada I, E.T.S. Ingenieros, Universidad del País Vasco, Alameda Urquijo s/n, E-48013 Bilbao, Spain. (ricardo.hueso@ehu.es; agustin.sanchez@ehu.es)

I. Khatuntsev and L. Zasova, Space Research Institute, Profsouznaya 84/32, Moscow, Russia. (nip@irn.iki.rssi.ru; zasova@irn.iki.rssi.ru)

A. Migliorini and G. Piccioni, Istituto di Astrofisica Spaziale e Fisica Cosmica, INAF-IASF Roma, Via del Foso del Cavaliere 100, I-00133 Rome, Italy. (alessandra.migliorini@iasf-roma.inaf.it; giuseppe.piccioni@iasf-roma.inaf.it)